ARTICLE

OPEN

Check for updates

Holocene extreme hydroclimate events in the Asian monsoon region were more frequent during cooler intervals

Enlou Zhang [1✉], Xianqiang Meng[1], Dongliang Ning[2], James Shulmeister [3], Weiwei Sun[1], Wenfang Zhang[1] & Zhenyu Ni[1]

The areas affected by the East and South Asian monsoons contain almost half the world's population. Understanding natural variability in these monsoons under warmer climates is critical for managing future changes. Here we present a high-resolution record of Holocene drought events derived from lake level changes in the South Asian monsoon region. By combining the published storm events in the East Asian monsoon region, we demonstrate that extreme hydroclimate events frequently occurred within a ca. 500-year cycle during the cool early-late Holocene, exhibiting a fierce Asian monsoon. In contrast, there were fewer extreme hydroclimate events during the warm mid-Holocene period. We propose that tropical temperatures and air-sea interaction in the Indo-Pacific Oceans are responsible for the occurrences of centennial-scale extreme events. Our findings suggest that tropical influences can module climate responses in monsoon regions, and the Asian monsoon may be more peaceful than hitherto expected under future global warming scenarios.

[1] State Key Laboratory of Lake Science and Environment, Nanjing Institute of Geography and Limnology, Chinese Academy of Sciences, Nanjing, China. [2] School of Geographic Science, Nantong University, Nantong, China. [3] School of Earth and Environment, University of Canterbury, Christchurch, New Zealand. ✉email: elzhang@niglas.ac.cn

Extreme hydroclimate events, primarily droughts and floods, have widespread impacts on economic and social development, as well as food security in the Asian monsoon regions. These regions consist of the South Asian monsoon and East Asian monsoon subsystems, which account for almost half of the population of the world[1,2]. It is therefore important to understand how extreme hydroclimate events in the Asian monsoon regions may change under expected future warming[2,3]. Projecting extreme hydroclimate events based on climate models is common in Asian monsoon regions under future global warming[2,4]. However, there are obvious uncertainties in simulating future extreme events using the current generation of models[5,6]. Scenario and model uncertainties lead to remarkable variability in projecting extreme precipitation[2,7]. Examining climate events during warm intervals in the recent geological past is a widely used approach to attempting to resolve these challenges[8,9].

The latest warm period, the Holocene, provides an opportunity to better understand the natural rhythm of extreme hydroclimate events in the Asian monsoon regions as well as their potential forcings[9,10]. Over the past several decades, paleoclimate studies have mainly focused on the sub-orbital scale Asian monsoon evolution over the Holocene[11–16]. It is generally accepted that the Asian monsoon was strong during the early to middle Holocene and then weakened[11–16]. However, the question of how centennial-scale extreme hydroclimate events have varied over the Holocene is still unclear due to the lack of high-resolution climate records from many areas[17,18]. Scattered paleoclimatic records from the East Asian monsoon have shown that extreme rainfall events occurred asynchronously with a 500-y quasi-periodicity in central and northeast China[19–21]. The scarcity of high-quality centennial-scale climate records from the South Asian monsoon domain limits the understanding of extreme hydroclimate events change across the wider Asian monsoon region.

The main reason for this deficiency is the poor sensitivity of existing records to extreme hydroclimate events. As widely used geological records for Asian monsoon intensity, $\delta^{18}O$ variation in stalagmite and lacustrine carbonate is predominately controlled by large-scale atmospheric circulation, which makes them only reliable for recording mean climate trends but not extreme events[22]. In tropical South Asian monsoon regions, where water availability is always enough for biological growth, frequently used biological proxies such as pollen have delayed responses and are relatively insensitive to centennial-scale climate events[23–25].

To address this, we present a continuous record of drought events during the Holocene based on lake level change from enclosed freshwater Lake Ximenglongtan (XMLT, 22°38′26″ N, 99°35′45″ E), which is located on the northeastern margin of the South Asian monsoon domain (Fig. 1). This record is well-constrained by radiocarbon dating using plant residues (Supplementary Fig. 1). Investigations of modern processes demonstrate that lake level changes are the dominant control on the distribution of the >32 μm% (GS32) of sediments. Further, comparison with modern instrument records was used to validate the sensitivity of lake level change to drought events for GS32 in sediment core dated by radionuclide ^{210}Pb and ^{137}Cs (Supplementary Fig. 2). By combining with published high-resolution extreme rainfall records from the East Asian monsoon regions, we investigate similarities and differences in the frequency and intensity of events and explore the phase relationship between extreme hydroclimate events in the two main Asian monsoon sub-regions. Finally, by comparing our results with tropical temperature variability and ocean-air interactions in the Indo-Pacific sectors, the potential mechanisms for extreme hydroclimate events are explored.

Results and discussion

Grain size indicates lake level change. Grain size sensitively records lake level change in this small enclosed lake. Generally, the near-shore shallow water zone has higher hydraulic energy than the off-shore deeper water zone, resulting in a ring-shaped distribution of grain size with fine grain fractions increasing from the near-shore to the lake center[26]. This was supported by modern investigation of Lake XMLT, which shows that finer grains deposit in the lake center and coarser sand grains settle at the lakeside (Fig. 2a). Therefore, when the lake level declines, the distance between the lakeside and lake center (our Holocene sediment core site) will decrease which facilitates the deposition of the larger grains in the lake center sediments. Therefore, grain size components are sensitive to lake water level variations. In contrast to the previous use of Holocene sedimentary cores to distinguish the grain size components sensitive to lake level changes[27], we apply a strategy that compares modern sediment distribution observations with past data to extract grain size components sensitive to water depth[13].

In this study, we present the >32 μm% grain-size fraction (GS32) of sediments from the lake center (deepest area) to resolve lake level changes based on the investigation of grain size in modern surficial sediments. The analysis of the grain size standard deviation in the surface sediments shows that measuring the percentage of particles larger than ~32 μm provides a sensitive indicator of lake depth (Fig. 2 and Supplementary Fig. 3). Nearly all particle sizes of the sediments are finer than 32 μm from the deep-water areas and coarser than 32 μm in shallow-water areas (Fig. 2a and Supplementary Fig. 3). This phenomenon is very similar to observations in our previous study[27] where >35.5 μm was used as the marker grain size. Further, a significant statistical correlation ($R^2 = 0.97$, $n = 28$, $p < 0.001$) between the GS32 and water depth also confirms that GS32 in the lake center sediment is a sensitive proxy of lake level changes with higher GS32 indicating lower lake water depth and shrinking lake area (Fig. 2d). The regression equation, lake water depth $(m) = -0.1859 \times GS32 + 17.56$ (EQ 1), can be used to predict lake level change.

Lake siltation also does change the grain size characteristics of sediments across the Holocene. However, we still conclude that the >32 μm component is insensitive to the ~10 m infilling of the lakebed since the early Holocene (Supplementary Fig. 1) based on several reasons. First, the offshore distance and slope also exert a primary influence on grain size changes. When the minimum offshore distance to the sample site is less than 130 m, the surface sediments' GS32 show a strong correlation with the minimum offshore distance (Fig. 2c), indicating a prominent slope input and local hydrodynamic control. However, beyond the threshold of 130 m, there is almost no correlation between the minimum offshore distance and GS32 in surface sediments (Fig. 2c). Similarly, in flat lakebeds with water depths exceeding 16 m, both GS32 and water depth exhibit a poor correlation (Supplementary Fig. 4). These findings suggest that GS32 is primarily sensitive in inshore areas. Second, when the lake reaches its maximum depth of 16–18 m, the GS32 value in the surficial sediments averages around 5.4%, which is approaching 0%. This observation implies that the GS32 value could not have been lower even at greater water depths (>18 m) that occurred during the early Holocene. Additionally, we utilize a threshold of 7% GS32 to identify extreme events during the Holocene, and this threshold is predominantly observed in lakebeds with water depths below 16 m rather than the deeper lakebed in modern sediments. These observations strengthen the conclusion that the GS32 value is not sensitive to variations in the deep water zone (>16 m) of Lake XMLT. Third, it is theoretically expected that lake siltation would lead to shallower water depths and coarser grain sizes. However, the median grain size data does not support a gradual trend of
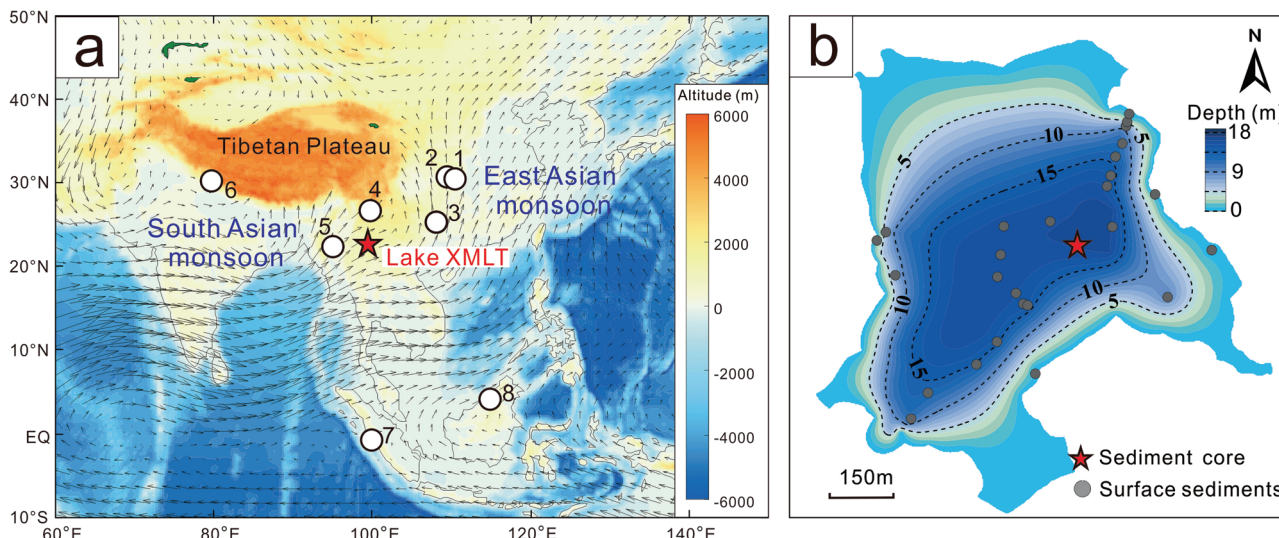
Fig. 1 Asian monsoon circulation and studied Lake XMLT. a Asian monsoon wind field at 850 hPa from May to September. The red star indicates the site of Lake XMLT, and the white circles indicate the sites of paleoclimatic records mentioned in the text. 1, Heshang Cave; 2, Xinya Cave; 3, Dongge Cave; 4, Lake Tiancai; 5, Lake Twintaung; 6, Pindar basin; 7, SO189-39KL; 8, BA03 stalagmite. **b** Bathymetry of Lake XMLT, the red star indicates the coring sampling site, and the gray circles indicate the sites of surface sediment samples.
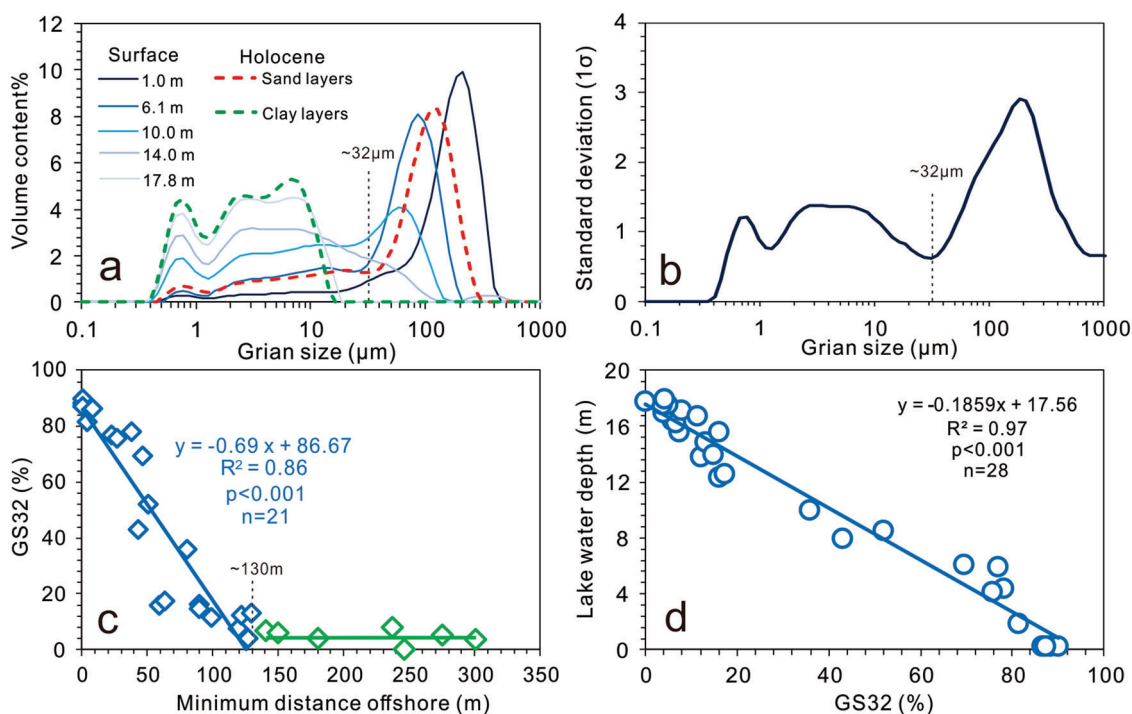

Fig. 2 Distribution of grain size at different lake water depths. a Distribution curve of grain size in modern surface sediments with different lake depths (solid curves) and Holocene sediments (dashed curves). **b** Standard deviation diagram of 28 surficial sediments at Lake XMLT. **c** The relation between minimum distance offshore (m) and GS32 (>32 μm%) in 28 surficial sediments (diamonds). Two classes were separated based on the minimum distance offshore of ~130 m. When the minimum distance offshore is lower than 130 m, the minimum distance offshore is very well correlated with GS32 (blue diamonds); in any case, there is no correlation (green diamonds). **d** Linear correlation between lake water depth and GS32 (>32 μm%) in 28 surficial sediments at Lake XMLT (circles).

coarsening (Supplementary Fig. 5) associated with the approximately 10-m siltation across the Holocene (Supplementary Fig. 1). This suggests that once the water depth reaches a certain level, potentially around 16 m, variations in grain size are primarily governed by offshore distance rather than lake depth. Therefore, EQ1 is primarily applicable for estimating the relative change of the lake drop concerning the outlet sites (the modern maximum water depth of 18 m and an elevation of 1140 m above sea level) rather than determining the absolute depth of the lake.

We believe that strong rainfall has limited influence on changes in the GS32 value of lake center sediments. First, as Lake XMLT is an enclosed freshwater lake, there is a threshold for the elevation of the highest lake level, which is consistent with the present lake level, even during a very strong rainfall event. During strong

rainfall, the isolation of the lake center makes it difficult for coarse sediments to reach the middle of the lake. This is supported by the sediment sizes in the lake center during modern high lake levels (Fig. 2). Second, while Lake XMLT has a perennial small inflow from its southwestern slope, there is no large stream entering the lake, and the dense vegetation cover in the catchment of Lake XMLT reduces the over-land transfer of coarse-grained soil from the slopes to the lake[27]. Third, there are no monitoring data on the change of the lake level in Lake XMLT, and the change of lake level is difficult to obtain through remote sensing due to the very small area and steep lake shore. However, a consistent trend between high GS32 and low lake levels is indirectly reflected by the regional meteorological data since AD 2002[28], including decreased mean annual precipitation, strong evapotranspiration, and low effective moisture (Fig. 3). Finally, the extraordinarily high GS32 in the Holocene sediments is often accompanied by plentiful of woody debris, which is only observed in the littoral deposits. Both sediment types strikingly resemble the characteristics of modern surface sediments in near-shore shallow-water areas.

In summary, the small catchment area and the high vegetation coverage in Lake XMLT limit the transportation of coarser particles from the catchment into the lake center during the high lake levels. It should be noted that the lake will overflow when the lake level exceeds its current level (18 m depth and 1140 m a.s.l), and thus the GS32 can not document the higher lake levels than the present. However, the peaks of GS32 content in core sediments undoubtedly capture the lower lake level intervals. Conbinations of the unique characteristics of the lakebed and surrounding catchment, as well as the investigations of modern deposition processes, strongly support the inference that GS32 in the lake center area is a sensitive proxy of low lake-level change.
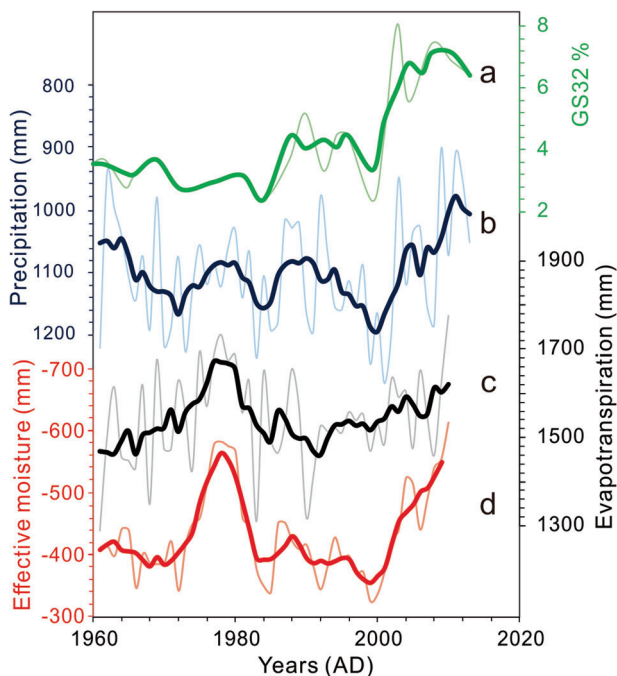

Fig. 3 Verification of geological GS32 record using instrumental record. Comparison between GS32 **a** from the sediment core at Lake XMLT constrained by [210]Pb–[137]Cs chronology (Supplementary Fig. 2) and regional instrumental data, including mean annual precipitation (**b**), evapotranspiration (**c**), and effective moisture from the difference between precipitation and evapotranspiration (**d**) since AD 1960 in Yunnan province, China[28]. The thick lines are values of 5 y of smoothing.

Holocene Asian monsoon extreme hydroclimate events. We defined Holocene extreme drought events in Lake XMLT using modern climate constraints. Regional average MAP in Yunnan Province based on meteorological stations declined from 1130 mm to 1050 mm from 1967 to 2002 AD[28] (Fig. 3). Similarly, the lake level declined by 0.6 m as indicated by GS32 in the sediment of Lake XMLT, which increased from 3.6% between 1967 and 2002 to 6.9% after 2002 (Fig. 3). In particular, well-described drought events happened between 2009 and 2012 AD[28,29], where MAP declined by approximately 15%, and GS32 increased to 7.1% compared with their average value between 1967 and 2002 (Fig. 3). Consequently, we used 7% of GS32 as a threshold for severe drought events during the Holocene. Namely, during the Holocene, only when GS32 exceeds 7%, we consider a severe drought event happened.

Based on the variation of GS32 from Lake XMLT sediments, we reconstruct the lake level change across the Holocene. We first estimate the lake water's maximum depth using the EQ1 and then calculate the lake level anomaly relative to the present maximum depth of ~18 m. The results show that three severe drought events were observed in the early Holocene at around 7.1, 7.5, and 8.0 cal ka BP, and five occurred at 0.3, 0.8, 1.6, 2.1, and 2.7 cal ka BP during the late Holocene (Fig. 4). These events were characterized by high GS32 values ranging between 21% and 76% with an average of 39%. The lake level is inferred to have dropped by an average of 10 ± 1.2 m ranging from 4 m to 14 m during these episodes. In contrast, almost all the GS32 values in the middle Holocene sediments are lower than 7%, and the dropping of lake level is lower than 2 m, indicating a relatively constant high lake level similar to the present. All these results indicate that frequent drought events occurred in the early and late Holocene, while drought events were rare during the middle Holocene. It should be noted that we have chosen to define the boundaries of the late, middle, and early Holocene as 3.0 ka and 7.0 ka, respectively. This differs from the 4.2 ka and 8.2 ka boundaries proposed by the Global Boundary Stratotype Section and Point. Our selection was motivated by the aim of better demonstrating the changes in extreme hydroclimate events within the Asian monsoon region.

Our observations are also supported by multiple paleoclimatic records in the South Asian monsoon region (Fig. 4). The chemical index of alteration (CIA) in Lake Tiancai indicates a frequent disturbance in chemical weathering after 3.0 cal ka BP, corresponding to more frequent cold and dry climate events during the late Holocene[30]. Similarly, the end-member modeling of Lake Bednikund in the central Himalayas[31] reveals that the content of coarse silt (EM1) reached peaks at ~2830–2610, ~1860–1050, ~760–580, and ~500–320 cal y BP. These peaks suggest abrupt declines in lake levels, which is nearly synchronous with the drought events documented in Lake XMLT (Fig. 4). Frequent extreme drought events during the late Holocene have also been observed in the southeastern Asian monsoon region through the pollen and biomarker records[32,33], and paleolimnological records in central India[34]. In contrast, all those proxies show less fluctuating climate conditions during the middle Holocene[30–33]. It is important to note that there may be some age discrepancies regarding the onset and duration of drought events, which may be attributable to dating uncertainties. Additionally, slight differences in the early Holocene among these records are possible due to variations in lake environments and the sensitivity of certain proxies to extreme events throughout the Holocene, particularly considering continuous sedimentation since the early Holocene. Nevertheless, the consistent evidence of frequent extreme hydroclimate events during the late Holocene, as recorded by various proxies in different regions, supports the notion that our GS32 record should be sensitive to reflecting such extreme events.
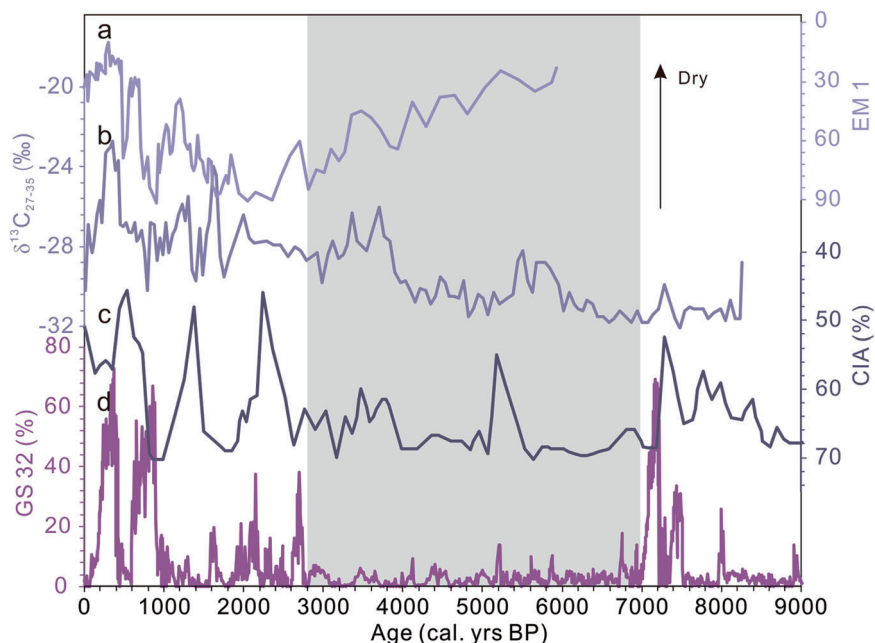
Fig. 4 Holocene extreme hydroclimate events in the South Asian monsoon regions. a Grain size end-members 1 of lake sediments from the central Himalaya[31]. **b** The $\delta^{13}C_{27-35}$ records from Lake Twintaung in Southeast Asia[32]. **c** Chemical alteration index (CIA) from Lake Tiancai, the northeast margin of the South Asian monsoon region[30]. **d** GS32 (>32 μm%) from Lake XMLT, the northeast margin of the South Asian monsoon region (this study).

Most importantly, the Holocene drought events inferred from the lake level changes at XMLT in the South Asian monsoon region align well with extreme rainfall events as derived from absolute-dated stalagmites in the distal East Asian monsoon region (Fig. 5a)[21]. Extreme rainfall events were indicated by $IRM_{soft-flux}$, the flux of isothermal remanent magnetization IRM_{soft}, which is traced to the variation in the flux of soil-derived magnetite particles per year[21]. Both results show that extreme rainfall events in central China and drought events in the South Asian monsoon region occurred frequently during the early and late Holocene (Fig. 5). There is also a remarkable 500-y periodicity in both records (Fig. 6). These coherences enhance the credibility of the reduced lake levels at Lake XMLT as the proxy for the regional severe drought events and enable us to further explore the relationships between the extreme hydroclimate events in the South Asian and East Asia monsoon regions.

It is noteworthy that the occurrence of drought events in the South Asian monsoon region is often associated with extreme rainfall events in central China, which is part of the East Asian monsoon region. During the early Holocene, there are generally synchronous peaks between extreme rainfall events in the East Asian monsoon region and severe drought events in the South Asian monsoon region centered at 7.1 and 8.0 cal ka BP (Fig. 5a). However, during the late Holocene after 3.0 cal ka BP, the phase relationship of extreme hydroclimate events in the two monsoon regions became complex and even out of phase. Due to the insensitivity of $IRM_{soft-flux}$ to drought events, we further compared our lake level changes with a high-resolution $\delta^{13}C$ record from a stalagmite in Xinya Cave, which is close to the Hesang Cave, Central China[35]. Drought occurred simultaneously around 0.3, 0.8, and 1.6 cal ka BP in both regions. In contrast, around 1.2 and 2.7 cal ka BP, both regions are antiphases (Fig. 7).

In summary, extreme hydroclimate events frequently occur with a ca. 500-y cycle during the early and late Holocene and are rare during the middle Holocene in the whole Asian monsoon region. The correlation in extreme hydroclimate events between the South Asian monsoon and central China East Asian monsoon is generally anti-phased during the early Holocene but complicated during the late Holocene.

Drivers of Asian monsoon extreme drought events during the Holocene. Ocean-air interactions in the tropical Indo-Pacific sectors, including the El Niño–Southern Oscillation (ENSO) and the Indian Ocean Dipole (IOD), and tropical temperature anomalies have synergistic effects on extreme hydroclimate events in the Asian monsoon regions[21,36–38]. Generally, during positive ENSO (El Niño phase) and positive IOD phases, there is an anomalous decreasing sea surface temperature gradient across the tropical Indo-Pacific sectors, which results in a weakened Walker circulation[38,39]. This, in turn, triggers an anomalous anticyclone extending from the tropical northwest Pacific to the eastern flank of the Tibetan Plateau, leading to drought conditions across most Asian monsoon areas and flooding in Central China[21,36,40]. Alternatively, negative ENSO (La Niña phase) and negative IOD will cause the opposite effect[21,36,40]. Therefore, an antiphase relationship in the extreme hydroclimate variability is usually observed between the South Asian monsoon and central China of the East Asian monsoon regions.

Many Holocene paleo-ENSO and IOD records support this hypothesis[41–45]. During the late Holocene, the $\delta^{18}O$ variances of fossil coral, foraminifera, and stalagmite support strengthened ENSO activity[42,43,45]. Lake deposits from Ecuador[41] and the Galapagos Islands[46] and model results[44] document strong ENSO during the late Holocene. Geological and climate model results (Fig. 3c)[41–45] also show a reduction in ENSO intensity during the middle Holocene. Intrashell oxygen isotope of sea shells from coastal southern Peru documented strong El Niño events during the early Holocene[47]. Although Holocene IOD records are very rare[48], IOD and ENSO have been frequently coupled over the last millennium[49] (Fig. 7d). Thus, we inferred the Holocene IOD is also a paired change to ENSO. The temperature gradient (ΔT) between surface sea temperature and thermocline temperature in western Sumatra was much higher after 3.0 ka BP, which reflects a more negative IOD mean state during the middle Holocene and
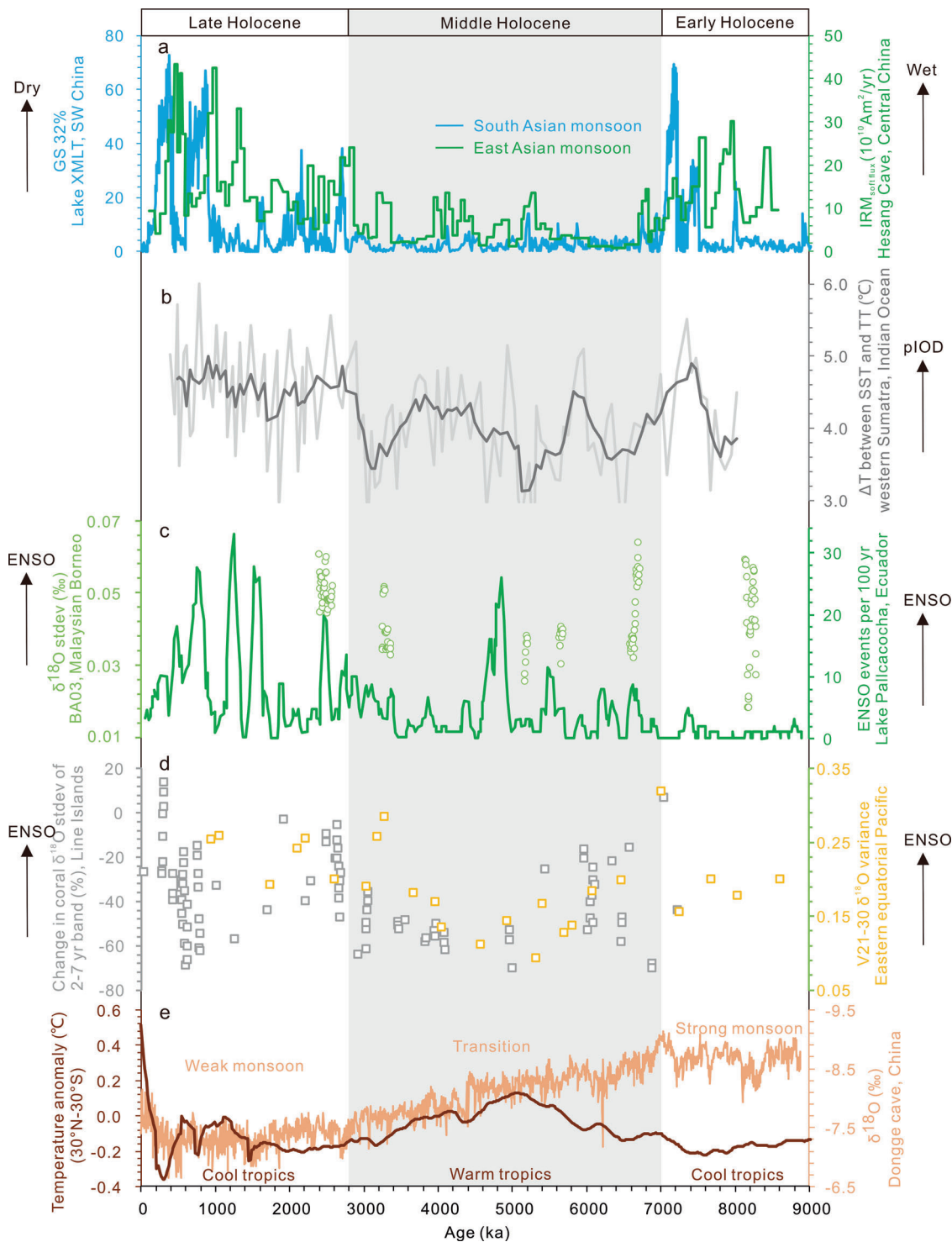
Fig. 5 Holocene Asian monsoon extreme hydroclimate events and related forcing. a Extreme hydroclimate events derived from the change in lake level at Lake XMLT in the South Asian monsoon region (ocean blue line, this study) and IRM_soft-flux of Hesang cave in the East Asian monsoon region (green line)[21]. Note that extreme hydroclimate events are opposed between East Asian monsoon and South Asian monsoon in the axis of ordinates. **b** Holocene Indian Ocean Dipole (IOD) change is indicated by the temperature gradient (ΔT) between surface sea temperature (SST) and thermocline temperature (TT) in western Sumatra, Indian Ocean[50]. The higher ΔT indicates a positive IOP-like state (pIOD). **c** ENSO changes are indicated by events per 100 y from sedimentation record in Laguna Pallcacocha, southern Ecuador (green line)[41] and stalagmite $\delta^{18}O$ estimates based on the standard deviation of the 2–7 y band in Malaysian Borneo, western Pacific warm pool[42]. **d** ENSO changes are indicated by the change in coral $\delta^{18}O$ stdev of the 2–7 y band in Line Islands[43] and Foraminiferal $\delta^{18}O$ variance in V21–30, Eastern Equatorial Pacific[45]. **e** Temperature anomaly in the tropics (red line)[54] and Asian monsoon intensity from stalagmite $\delta^{18}O$ in Dongge cave (green line)[12]. The vertical band indicates the mid-Holocene warm period.

a more positive IOD mean state during the late Holocene (Fig. 5b)[50]. Although the amplitude of ΔT changes was larger before 3.0 ka BP, a relatively steady negative IOD mean state during the middle Holocene might have enhanced the South Asian monsoonal precipitation and limited the occurrence of drought events. During the late Holocene, largely positive IOD conditions especially superimposed with the high-frequency fluctuations, should have facilitated the frequent occurrence of drought events. Additionally, due to the limited record length, it is challenging to fully capture the IOD signal covering the entire early Holocene. However, during the 7–7.5 ka period, ΔT is

slightly higher than that (it has a maximum of 5.5 °C) of the mid-Holocene (maximum of 5.0 °C)[50]. Therefore, we inferred that the IOD exhibited a positive phase during the early and late Holocene periods, which favored the occurrence of extreme hydroclimate events in the Asian monsoon region. In summary, although there are still discrepancies regarding the paleo-ENSO and IOD variabilities, it is generally agreed that the ENSO and IOD variabilities are strong during the early and late Holocene and weak during the middle Holocene[41–47].

The strong ENSO and IOD variabilities during the early and late Holocene are consistent with the frequent occurrence of extreme hydroclimate events in the Asian monsoon region. Frequent occurrence of drought events in the South Asian monsoon region and extreme rainfall events in central China of the East Asian monsoon region during the early and late Holocene also support the effect of ENSO and IOD on extreme hydroclimate events in the Asian monsoon region (Fig. 5d). The weak ENSO and IOD variabilities during the middle Holocene correspond to a reliable but quiescent Asian monsoon (Fig. 5d). Furthermore, ~500 y cycles of both extreme hydroclimate events in both Asian monsoon regions (Fig. 6) are also consistent with the cycles of Holocene modeled ENSO activity[44]. Although there are ~500-y solar cycles that fit our periodicity, it is hard to explain the quiescent Asian monsoon during the middle Holocene[51].

In this context, special attention should be paid to the contemporaneous drought events that occurred in both Asian monsoon sub-regions after 3.0 cal ka BP (Fig. 7). This phenomenon cannot be simply explained by the variability of
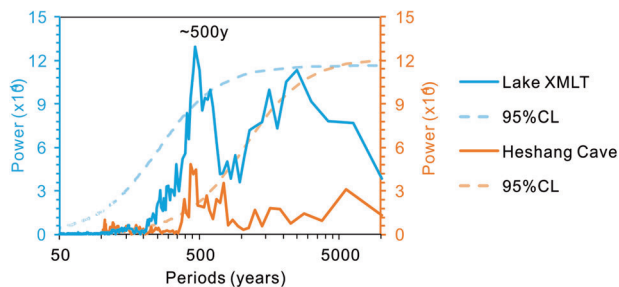

Fig. 6 Approximately 500 y-cycle of extreme hydroclimate events. Power spectrum analysis of lake level changes at Lake XMLT from the South Asian monsoon region (blue lines, this study) and IRMsoft-flux of Hesang Cave from the East Asian monsoon region (orange lines)[21]. Dashed lines have a 95% confidence level (CL). Only the ~500-y peak exceeds 95% confidence.
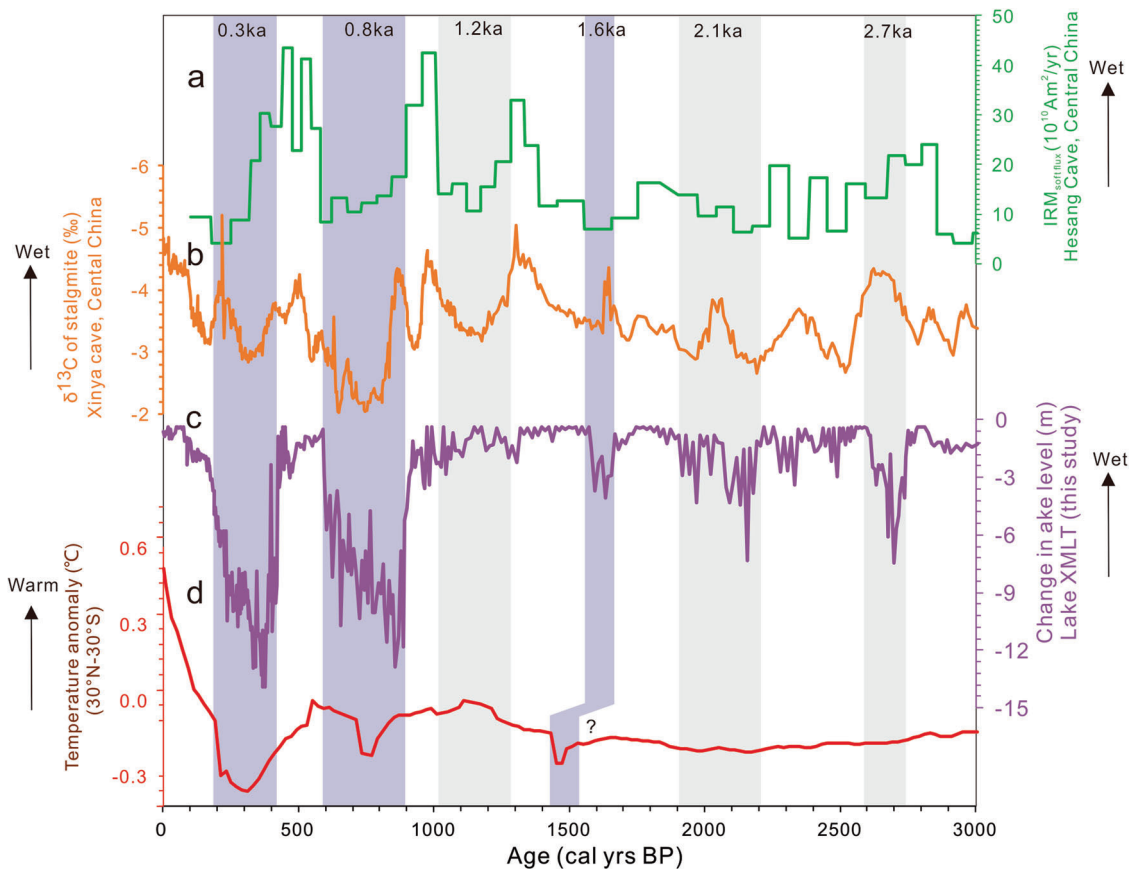

Fig. 7 Asian monsoon extreme hydroclimate events and tropical temperature change since 3 cal ka BP. a Storm events recorded by IRMsoft-flux of Hesang cave in Central China of East Asian monsoon region[21]. **b** Extreme hydroclimate events documented by $\delta^{13}C_{stalagmite}$ record from Xinya Cave, Central China of East Asian monsoon region[35]. **c** Extreme drought events derived from the change in lake level at Lake XMLT in the South Asian monsoon region (this study). **d** Temperature anomaly in the tropics (red line)[54]. The light blue vertical bands indicate drought events, and the gray vertical bands indicate the opposite phase of extreme hydroclimate events between two Asian monsoon sub-regions.

ocean–air interactions in the tropical Indo-Pacific, which would result in an antiphase relation in the extreme hydroclimate conditions in both monsoon sub-regions[21,36,40]. For instance, strong ENSO and IOD at 0.3 and 0.8 ka inferred by moving 30-y standard deviations of coral $\delta^{18}O$[43,49] should cause drought in Lake XMLT of the South Asian monsoon region and extreme rainfall in both Xinya and Hesang caves in Central China, while Central China yields a drought signal at this time (Fig. 7). Therefore, air-sea interactions alone cannot fully explain extreme climatic events in the Holocene.

In addition to air–sea interactions, we propose that tropical temperature change also plays an important role in extreme hydroclimate events[13,52]. Clausius–Clapeyron equation states that a 7% increase in integrated water vapor for every degree Celsius results in a 2–3% increase in precipitation, subject to energetic constraints. This means that lower temperatures will decrease atmospheric moisture and precipitation significantly[53]. The co-occurrence of drought events in both Asian monsoon sub-regions around 1.6, 0.8, and 0.3 cal ka BP is closely associated with cool phases in the tropics[54] (Fig. 7). Across the Holocene, warm tropics during the middle Holocene also correlates to a quiescent Asian monsoon and cool tropics during the early and late Holocene correlates to a fierce Asian monsoon (Fig. 5). Our findings do not entirely align with future global warming projections, which anticipate an increase in the frequency of extreme hydroclimate events in the Asian monsoon regions[2,4]. Our observations may indicate climate responses responsible for uncertainties in the model[7], or there may be a differential response of extreme hydroclimate events to natural warming as opposed to human-induced warming caused by anthropogenic CO_2 emissions[2].

In summary, the overall pattern of active extreme hydroclimate events in the early and late Holocene with cool tropics and suppressed variability during the middle Holocene with warm tropics in Asian monsoon regions. We also found that extreme hydroclimate events frequently occurred during constant strong or weak monsoon intensity (early and late Holocene) rather than during the transition period from strong to weak monsoon in the middle Holocene (Fig. 5). We propose that Holocene extreme hydroclimate events in the Asian monsoon region have been primarily controlled by ocean–atmosphere interactions in the tropical Indo-Pacific and the tropical temperature. Our findings also suggest that extreme hydroclimate events occur mainly in cool periods rather than warm periods, which may provide a natural benchmark for the occurrence of extreme hydroclimate events under future global warming scenarios.

Materials and methods
The setting of Lake XMLT. Lake XMLT is located in the southeastern Yunnan province, China (Fig. 1), which is particularly drought-impacted[55]. The climate around Lake XMLT is strongly controlled by the South Asian monsoon. It is a small enclosed lake with a surface area of only ~0.5 km² and a maximum water depth of 18 m and 1140 m above sea level (a.s.l). Lake XMLT is hydrologically recharged through precipitation, surface runoff, and a perennial small stream on its southwestern slope[27]. Most rainfall (90%) occurs during the wet season between May and October[27]. With a steep and small catchment, the lake is very sensitive to high-frequency climate oscillations. The catchment of Lake XMLT is somewhat protected from erosion because of the dense vegetation cover[27].

In July 2013, a 10.6 m sediment core (XMLT-1) was extracted from the depocenter using a piston sampler on the UWITEC platform system. The sediment core was subsequently sectioned at 1 cm intervals and stored at ~4 °C for further analysis.

However, due to the potential disturbance and contamination of the surface sediment during the sampling process using a piston sampler, we also collected a 30 cm gravity core (XMLT-2) near XMLT-1. This reference core was collected using a gravity corer and served to validate the reliability of the geological record by comparing it with instrumental records. XMLT-2, which is 30 cm long, was collected from a location 3 m away from the Holocene core XMLT-1. The sediment core XMLT-2 was subsequently sectioned at 0.5 cm intervals for grain size analysis.

Chronology of sediment cores in Lake XMLT. The chronology was established using accelerator mass spectrometry ^{14}C dating of plant materials. Twelve terrestrial plant fragments picked from different depths of the core were analyzed at the Beta Analytic Radiocarbon Dating Laboratory, as reported in our previous study[27]. In this study, to improve age precision, the newly published IntCal 20 calibration dataset[56] was applied to calibrate the age-depth curves using raw ^{14}C age data[27,56]. After calibrated to calendar years BP (0 BP = AD 1950), the dating results were interpolated using a Bayesian model in the Bacon program implemented in R 3.1.0 with default settings for lake sediments[57] to acquire the age-depth model (Supplementary Fig. 1). The final calculated basal age of the core is ~9.4 cal ka BP with an average deposition rate of 0.11 cm/y, which is similar to the previous dating results[27].

The chronology of core XMLT-2 was established by radionuclide ^{210}Pb and ^{137}Cs data, which were determined at every 0.5 cm interval with a gamma spectrometer (Hyperpure Ge detector) at 0.5 cm intervals (Supplementary Fig. 2)[58]. The results show that total ^{210}Pb ($^{210}Pb_{total}$) activity decreased exponentially with depth. Equilibrium between $^{210}Pb_{total}$ and ^{226}Ra activities was reached at the bottom of the sediment core. The ^{137}Cs peak at 9 cm depth in the core should correspond to 1963AD, which has the maximum nuclear weapon testing peak[58]. The decline of excess ^{210}Pb ($^{210}Pbex$) activity in the core follows an approximate exponential trend with depth indicating its constant supply rate. So, a constant rate of supply model, not a constant initial concentration (CIC) model, was used for the chronology construction. In addition, 28 surficial sediment samples were acquired from across the lake to understand the sedimentation processes, which highlighted the relationship between the grain size and lake depth (Fig. 1).

Measurement of grain size. The grain size of sediments was measured at 1-cm intervals (a total of 1050 samples) for the Holocene XMLT-1 sediment core, at 0.5-cm intervals for the XMLT-2 sediment core (a total of 18 samples), and the modern surface samples (a total of 28 samples). It should be noted that the grain size data in odd samples for the Holocene sediment core (total of 526 samples) has been reported in our previous work[27], measured by the old Malvern Mastersizer 2000 laser particle sizer. In order to maintain uniform and comparable grain size data, we measured the grain size of all samples using the newer Malvern Mastersizer 3000 laser particle sizer. Before measurement, the organic matter and carbonates in samples are removed using H_2O_2 and HCl, respectively. So, the analysis results only present the grain size distribution of the clastic fractions. All the samples were dispersed in an ultrasonic bath for 15 min after the addition of $(NaPO_3)_6$. Each sample was measured three times, and the three results needed to be highly similar to be considered qualified. A final average value of three times was obtained to reduce the measurement errors. In addition, power spectral analyses of extreme hydroclimate event records in Asian monsoon regions were carried out using PAST3.0 REDFIT software, providing valuable insights into the temporal patterns and frequency

distribution of these events. Firstly, data are imported into the Past3.0 software, and oversampling and segmentation values (e.g., 2 oversamples and 2 segments) are set. After setting up the parameters and configurations, the power spectral analysis utilizing the REDFIT algorithm was executed.

Data availability

References

1. Wang B. *The Asian Monsoon*. (Springer, 2006).
2. IPCC. Climate change 2021: the physical science basis. (2021).
3. Dai, A. Drought under global warming: a review. *WIREs Clim. Change* **2**, 45–65 (2011).
4. Cai, W. et al. Increased frequency of extreme Indian Ocean Dipole events due to greenhouse warming. *Nature* **510**, 254–258 (2014).
5. Emile-Geay, J. et al. Links between tropical Pacific seasonal, interannual and orbital variability during the Holocene. *Nat. Geosci.* **9**, 168 (2015).
6. Douville, H. et al. Water Cycle Changes. In Climate Change 2021. In: *The Physical Science Basis. Contribution of Working Group I to the Sixth Assessment Report of the Intergovernmental Panel on Climate Change* (eds Masson-Delmotte V, P. Zhai, A. Pirani, S. L. Connors, C. Péan, S. Berger N. C., Y. Chen, L. Goldfarb, M. I. Gomis, M. Huang, K. Leitzell, E. Lonnoy, J. B. R. Matthews, T. K., Maycock T. W., O. Yelekçi, R. Yu, and B. Zhou) (2021).
7. Zhou, T., Lu, J., Zhang, W. & Chen, Z. The sources of uncertainty in the projection of global land monsoon precipitation. *Geophys. Res. Lett.* **47**, e2020GL088415 (2020).
8. Mohtadi, M., Prange, M. & Steinke, S. Palaeoclimatic insights into forcing and response of monsoon rainfall. *Nature* **533**, 191–199 (2016).
9. Tierney, J. E. et al. Past climates inform our future. *Science* **370**, eaay3701 (2020).
10. Mayewski, P. A. et al. Holocene climate variability. *Quat. Res.* **62**, 243–255 (2004).
11. Chen, F. et al. East Asian summer monsoon precipitation variability since the last deglaciation. *Sci. Rep.* **5**, 1–11 (2015).
12. Wang, Y. et al. The Holocene Asian monsoon: links to solar changes and North Atlantic climate. *Science* **308**, 854–857 (2005).
13. Zhang, E. et al. Millennial-scale hydroclimate variations in southwest China linked to tropical Indian Ocean since the Last Glacial Maximum. *Geology* **45**, 435–438 (2017).
14. Lu, H. et al. Variation of East Asian monsoon precipitation during the past 21 ky and potential CO2 forcing. *Geology* **41**, 1023–1026 (2013).
15. Goldsmith, Y. et al. Northward extent of East Asian monsoon covaries with intensity on orbital and millennial timescales. *Proc. Natl Acad. Sci. USA* **114**, 1817–1821 (2017).
16. Zhou, X. et al. Monthly insolation linked to the time-transgressive nature of the Holocene East Asian monsoon precipitation maximum. *Geology* **50**, 331–335 (2021).
17. Li, Y., Wang, N., Zhou, X., Zhang, C. & Wang, Y. Synchronous or asynchronous Holocene Indian and East Asian summer monsoon evolution: a synthesis on Holocene Asian summer monsoon simulations, records and modern monsoon indices. *Glob. Planet. Change* **116**, 30–40 (2014).
18. Liu, J. et al. Holocene East Asian summer monsoon records in northern China and their inconsistency with Chinese stalagmite δ18O records. *Earth Sci. Rev.* **148**, 194–208 (2015).
19. Xu, D. et al. Asynchronous 500-year summer monsoon rainfall cycles between Northeast and Central China during the Holocene. *Glob. Planet. Change* **195**, 103324 (2020).
20. Chu, G. et al. Holocene cyclic climatic variations and the role of the Pacific Ocean as recorded in varved sediments from northeastern China. *Quat. Sci. Rev.* **102**, 85–95 (2014).
21. Zhu, Z. et al. Holocene ENSO-related cyclic storms recorded by magnetic minerals in speleothems of central China. *Proc. Natl Acad. Sci. USA* **114**, 852–857 (2017).
22. Cheng, H. et al. Orbital-scale Asian summer monsoon variations: paradox and exploration. *Sci. China Earth Sci.* **64**, 529–544 (2021).
23. Cheng, J. et al. Vegetation feedback causes delayed ecosystem response to East Asian Summer Monsoon Rainfall during the Holocene. *Nat. Commun.* **12**, 1843 (2021).
24. Xu, P. et al. Diverse responses of different structured forest to drought in Southwest China through remotely sensed data. *Int. J. Appl. Earth Observ. Geoinf.* **69**, 217–225 (2018).
25. Niu, S. et al. Plant growth and mortality under climatic extremes: an overview. *Environ. Exp. Bot.* **98**, 13–19 (2014).
26. Last, W. M. & Smol, J. P. Tracking environmental change using lake sediments. 2. Physical and geochemical methods. Tracking environmental change using lake sediments. 2. Physical and geochemical methods (2001).
27. Ning, D., Zhang, E., Sun, W., Chang, J. & Shulmeister, J. Holocene Indian Summer Monsoon variation inferred from geochemical and grain size records from Lake Ximenglongtan, southwestern China. *Palaeogeogr. Palaeoclimatol. Palaeoecol.* **487**, 260–269 (2017).
28. Ji, Z., Huang, Z. & Xie, G. Dry-wet climate change in Yunnan during 1961–2010 (In Chinese with English abstract). *Meteorol. Sci. Technol.* **41**, 1073–1079 (2013).
29. Yan, Z., Zhang, Y., Zhou, Z. & Han, N. The spatio-temporal variability of droughts using the standardized precipitation index in Yunnan, China. *Nat. Hazards* **88**, 1023–1042 (2017).
30. Chen, X. et al. Direct and indirect effects of Holocene climate variations on catchment and lake processes of a treeline lake, SW China. *Palaeogeogr. Palaeoclimatol. Palaeoecolo.* **502**, 119–129 (2018).
31. Rawat, V. et al. Middle Holocene Indian summer monsoon variability and its impact on cultural changes in the Indian subcontinent. *Quat. Sci. Rev.* **255**, 106825 (2021).
32. Chu, G. et al. Drought cycles over the last 8, 200 years recorded in Maar lake Twintaung, Myanmar. *J. Geophys. Res.* **n/a**, e2019JD032225 (2020).
33. Dubois, N. et al. Indonesian vegetation response to changes in rainfall seasonality over the past 25,000 years. *Nat. Geosci.* **7**, 513–517 (2014).
34. Prasad, S. et al. Prolonged monsoon droughts and links to Indo-Pacific warm pool: a Holocene record from Lonar Lake, central India. *Earth Planet. Sci. Lett.* **391**, 171–182 (2014).
35. Li, J.-Y. et al. High-resolution δ18O and δ13C records of an AMS 14C and 230Th/U dated stalagmite from Xinya Cave in Chongqing: Climate and vegetation change during the late Holocene. *Quat. Int.* **447**, 75–88 (2017).
36. Hernández, A. et al. Modes of climate variability: synthesis and review of proxy-based reconstructions through the Holocene. *Earth Sci. Rev.* **209**, 103286 (2020).
37. Krishnaswamy, J. et al. Non-stationary and non-linear influence of ENSO and Indian Ocean Dipole on the variability of Indian monsoon rainfall and extreme rain events. *Clim. Dyn.* **45**, 175–184 (2015).
38. Cane, M. A. & Zebiak, S. E. A theory for El Niño and the Southern Oscillation. *Science* **228**, 1085–1087 (1985).
39. Cane, M. A. The evolution of El Niño, past and future. *Earth Planet. Sci. Lett.* **230**, 227–240 (2005).
40. Li, X. & Ting, M. Recent and future changes in the Asian monsoon-ENSO relationship: natural or forced? *Geophys. Res. Lett.* **42**, 3502–3512 (2015).
41. Moy, C. M., Seltzer, G. O., Rodbell, D. T. & Anderson, D. M. Variability of El Niño/Southern Oscillation activity at millennial timescales during the Holocene epoch. *Nature* **420**, 162 (2002).
42. Chen, S. et al. A high-resolution speleothem record of western equatorial Pacific rainfall: implications for Holocene ENSO evolution. *Earth Planet. Sci. Lett.* **442**, 61–71 (2016).
43. Cobb, K. M. et al. Highly variable El Niño–Southern oscillation throughout the holocene. *Science* **339**, 67–70 (2013).
44. Liu, Z. et al. Evolution and forcing mechanisms of El Nino over the past 21,000 years. *Nature* **515**, 550–553 (2014).
45. Koutavas, A. & Joanides, S. El Niño–Southern Oscillation extrema in the Holocene and Last Glacial Maximum. *Paleoceanography* **27**, PA4208 (2012).
46. Conroy, J. L., Overpeck, J. T., Cole, J. E., Shanahan, T. M. & Steinitz-Kannan, M. Holocene changes in eastern tropical Pacific climate inferred from a Galápagos lake sediment record. *Quat. Sci. Rev.* **27**, 1166–1180 (2008).
47. Carrè, M., Bentaleb, I., Fontugne, M. & Lavallee, D. Strong El Niño events during the early Holocene: stable isotope evidence from Peruvian sea shells. *Holocene* **15**, 42–47 (2005).
48. Abram, N. J. et al. Palaeoclimate perspectives on the Indian Ocean Dipole. *Quat. Sci. Rev.* **237**, 106302 (2020).
49. Abram, N. J. et al. Coupling of Indo-Pacific climate variability over the last millennium. *Nature* **579**, 385–392 (2020).
50. Kwiatkowski, C. et al. Holocene variations of thermocline conditions in the eastern tropical Indian Ocean. *Quat. Sci. Rev.* **114**, 33–42 (2015).
51. Damon, P. E. & Jirikowic, J. L. The Sun as a Low-Frequency Harmonic Oscillator. *Radiocarbon* **34**, 199–205 (1992).
52. Tierney, J. E., Pausata, F. S. R. & deMenocal, P. Deglacial Indian monsoon failure and North Atlantic stadials linked by Indian Ocean surface cooling. *Nat. Geosci.* **9**, 46–50 (2016).

53. Allan, R. P. et al. Physically Consistent Responses of the Global Atmospheric Hydrological Cycle in Models and Observations. *Surv. Geophys.* **35**, 533–552 (2014).

54. Marcott, S. A., Shakun, J. D., Clark, P. U. & Mix, A. C. A reconstruction of regional and global temperature for the Past 11,300 years. *Science* **339**, 1198–1201 (2013).

55. Christian, J. I. et al. Global distribution, trends, and drivers of flash drought occurrence. *Nat. Commun.* **12**, 6330 (2021).

56. Reimer, P. J. et al. The IntCal20 northern hemisphere radiocarbon age calibration curve (0–55 cal kBP). *Radiocarbon* **62**, 725–757 (2020).

57. Blaauw, M. & Christen, J. A. Flexible paleoclimate age-depth models using an autoregressive gamma process. *Bayesian Anal.* **6**, 457–474 (2011). 418.

58. Appleby P. G. Chronostratigraphic techniques in recent sediments. *Tracking environmental change using lake sediments: basin analysis, coring, and chronological techniques*, (Kluwer Academic Publishers, 2001).

Author contributions

E.Z. and X.M. conceived this research. X.M. and D.N. performed laboratory analyses and analysis of the data. X.M., D.N., and E.Z. wrote the manuscript with significant contributions by J.S. W.S., W.Z., and Z.N. contributed to the discussion of results. All authors interpreted the results.

Competing interests

The authors declare no competing interests.

Additional information

Supplementary information The online version contains supplementary material available at https://doi.org/10.1038/s43247-023-00997-x.

Correspondence and requests for materials should be addressed to Enlou Zhang.

Peer review information *Communications Earth & Environment* thanks Inka Meyer and the other anonymous reviewer(s) for their contribution to the peer review of this work. Primary Handling Editors: Ola Kwiecien, Heike Langenberg, Alienor Lavergne. A peer review file is available.

Reprints and permission information is available at http://www.nature.com/reprints

Publisher's note Springer Nature remains neutral with regard to jurisdictional claims in published maps and institutional affiliations.

Terms and Conditions

Springer Nature journal content, brought to you courtesy of Springer Nature Customer Service Center GmbH ("Springer Nature").

Springer Nature supports a reasonable amount of sharing of research papers by authors, subscribers and authorised users ("Users"), for small-scale personal, non-commercial use provided that all copyright, trade and service marks and other proprietary notices are maintained. By accessing, sharing, receiving or otherwise using the Springer Nature journal content you agree to these terms of use ("Terms"). For these purposes, Springer Nature considers academic use (by researchers and students) to be non-commercial.

These Terms are supplementary and will apply in addition to any applicable website terms and conditions, a relevant site licence or a personal subscription. These Terms will prevail over any conflict or ambiguity with regards to the relevant terms, a site licence or a personal subscription (to the extent of the conflict or ambiguity only). For Creative Commons-licensed articles, the terms of the Creative Commons license used will apply.

We collect and use personal data to provide access to the Springer Nature journal content. We may also use these personal data internally within ResearchGate and Springer Nature and as agreed share it, in an anonymised way, for purposes of tracking, analysis and reporting. We will not otherwise disclose your personal data outside the ResearchGate or the Springer Nature group of companies unless we have your permission as detailed in the Privacy Policy.

While Users may use the Springer Nature journal content for small scale, personal non-commercial use, it is important to note that Users may not:

1. use such content for the purpose of providing other users with access on a regular or large scale basis or as a means to circumvent access control;

2. use such content where to do so would be considered a criminal or statutory offence in any jurisdiction, or gives rise to civil liability, or is otherwise unlawful;

3. falsely or misleadingly imply or suggest endorsement, approval , sponsorship, or association unless explicitly agreed to by Springer Nature in writing;

4. use bots or other automated methods to access the content or redirect messages

5. override any security feature or exclusionary protocol; or

6. share the content in order to create substitute for Springer Nature products or services or a systematic database of Springer Nature journal content.

In line with the restriction against commercial use, Springer Nature does not permit the creation of a product or service that creates revenue, royalties, rent or income from our content or its inclusion as part of a paid for service or for other commercial gain. Springer Nature journal content cannot be used for inter-library loans and librarians may not upload Springer Nature journal content on a large scale into their, or any other, institutional repository.

These terms of use are reviewed regularly and may be amended at any time. Springer Nature is not obligated to publish any information or content on this website and may remove it or features or functionality at our sole discretion, at any time with or without notice. Springer Nature may revoke this licence to you at any time and remove access to any copies of the Springer Nature journal content which have been saved.

To the fullest extent permitted by law, Springer Nature makes no warranties, representations or guarantees to Users, either express or implied with respect to the Springer nature journal content and all parties disclaim and waive any implied warranties or warranties imposed by law, including merchantability or fitness for any particular purpose.

Please note that these rights do not automatically extend to content, data or other material published by Springer Nature that may be licensed from third parties.

If you would like to use or distribute our Springer Nature journal content to a wider audience or on a regular basis or in any other manner not expressly permitted by these Terms, please contact Springer Nature at

onlineservice@springernature.com